Electronic Supplementary Material (ESI) for ChemComm.

Supporting Information

In-situ Self-transformation of Small Gold Clusters to Gold Nanocrystals Toward Boosted Photoreduction Catalysis

Ming-Hui Huang, [a] Xiao-Cheng Dai, [a] Tao Li, [a] Yu-Bing Li, [a] Shuo Hou, [a] Yunhui He, [b] Guangcan Xiao, [b] Fang-Xing Xiao* [a]

a. College of Materials Science and Engineering, Fuzhou University, New Campus, Minhou, Fujian Province 350108, China.

b. Instrumental Measurement and Analysis Center, Fuzhou University, Fuzhou, 350002, People's Republic of China.

Email: fxxiao@fzu.edu.cn

1. Experimental section.

1.1 Materials

Cadmium chloride ($CdCl_2 \cdot 2.5H_2O$), sodium borohydride ($NaBH_4$), sodium hydroxide (NaOH), mercaptoacetic acid (MAA), ethylenediamine ($C_2H_8N_2$), ethanol (C_2H_6O), sulfuric acid (H_2SO_4), potassium peroxodisulfate ($K_2S_2O_8$), sodium sulfite (Na_2SO_3), nitric acid (HNO_3), hydrochloric acid (HCl), 30% hydrogen peroxide (H_2O_2), potassium permanganate ($KMnO_4$), phosphorus pentoxide (P_2O_5), and graphite powder were obtained from Sinopharm Chemical Reagent Co., Ltd. (Shanghai, China). Selenium (Se) powder, gold (III) chloride trihydrate ($HAuCl_4 \cdot 3H_2O$), 4-nitroaniline (4-NA), 3-nitroaniline (3-NA), 2-nitroaniline (2-NA), 4-nitrophenol (4-NP), 3-nitrophenol (3-NP), 2-nitrophenol (2-NP), 4-nitrotoluene, and 4-nitroanisole were obtained from Aladdin Industrial Corporation (Shanghai, China). *N*-ethyl-*N'*-(3-dimethylaminopropyl) carbodiimide methiodide (EDC, 98%) and Deionized water (DI H_2O, Millipore, 18.2 MΩ cm resistivity) were obtained from Alfa Aesar (China) Chemicals Co., Ltd. L-glutathione reduced ($C_{10}H_{17}N_3O_6S$, GSH) was obtained from Sigma-Aldrich. All the materials above were used directly without further purification.

1.2 Preparation of MAA-capped CdSe QDs

CdSe QDs were synthesized based on an aqueous synthesis method reported previously with some modifications. Specifically, 2 mmol of $CdCl_2 \cdot 2.5H_2O$ was dissolved in 200 mL of DI H_2O and deaerated with N_2 bubbling in a three-necked flask for 1 h. After that, 230 μL of MAA, as a stabilizer, was added into above solution. The pH value of mixture was adjusted to 11 with 1 M NaOH aqueous solution. Subsequently, oxygen-free NaHSe aqueous solution was prepared by dissolving 0.6320 g of $NaBH_4$ in 10 mL of DI H_2O under N_2 bubbling, into which 0.2106 g of Se powder was added and stirred at a low speed for 2 h in an ice bath. 5 mL of the freshly prepared NaHSe aqueous solution was

quickly injected into Cd^{2+} aqueous solution under vigorous stirring and an orange-red solution was obtained and then it was refluxed in 333 K for 4 h. After cooling down to room temperature, the as-prepared CdSe QDs aqueous solution was precipitated by adding into equal volume of ethanol with vigorous stirring, the precipitated CdSe QDs was separated by centrifugation and dried in vacuum at 313 K.

1.3 Preparation of graphene oxide (GO)

Graphene oxide (GO) was synthesized from natural graphite powder by a modified Hummers method. In detail, 2 g of graphite powder was put into a mixture of 12 mL of concentrated H_2SO_4, 2.5 g of $K_2S_2O_8$, and 2.5 g of P_2O_5. The solution was heated to 80℃ in an oil bath kept stirring for 24 h. The mixture was then carefully diluted with 500 mL of deionized (DI) water, filtered, and washed until the pH of rinse water became neutral. The product was dried under ambient condition overnight. This pre-oxidized graphite was then subjected to oxidation described as follows. In a typical procedure, pre-oxidized graphite powder was added to a mixture of 120 mL of concentrated H_2SO_4 and 30 mL of HNO_3 under vigorous stirring, and the solution was cold to 0℃. Then, 15 g of $KMnO_4$ was added gradually under stirring, and the temperature of the mixture was kept to be below 20℃ by cooling. Successively, the mixture was stirred at room temperature for 96 h and then diluted with 1 L of DI water in an ice bath to keep the temperature below 50℃ for 2 h. Shortly after the further dilution with 1 L of DI water, 20 mL of 30% H_2O_2 was then added to the mixture, and a brilliant yellow product was formed along with bubbling. The mixture was filtered and washed with 1:10 HCl aqueous solution to remove metal ions followed by DI water to remove the acid. The filter cake was then dispersed in water by a mechanical agitation. Low-speed centrifugation was done at 1000 rpm for 2 min. The supernatant then underwent two more high-speed centrifugation steps at 8000 rpm for 15 min to

remove small GO pieces and water-soluble byproduct. The final sediment was re-dispersed in water with mechanical agitation or mild sonication using a table-top ultrasonic cleaner, giving a solution of exfoliated GO. The GO separated and dried is in the form of a brown powder.

1.4 Preparation of positively charged graphene oxide (GO)

GO was synthesized by a modified Hummer method. Preparation of positively charged GO was referred to a previous work.[49] Specifically, 50 mg of GO was dissolved in 100 mL of DI H_2O with ultrasonication for several hours. Then, 0.625 g of EDC and 5 mL of ethylenediamine was added into 50 mL of GO aqueous suspension, followed by uninterruptedly stirring at ambient conditions for 12 h. The resulting suspension was dialyzed (molecular weight cut-off, 12-14kD, Spectra/Por) for 3 days to remove the residual EDC and ethylenediamine.

1.5 Synthesis of L-glutathione-capped Au_x clusters

Gold (III) chloride trihydrate (40 mg) and L-glutathione (GSH, 46 mg) were thoroughly mixed in 50 mL of DI H_2O at ambient conditions. The mixture was continuously stirred until the appearance of a colorless solution and then heated at 323 K for 24 h. The Au_x clusters aqueous solution was stored at 4℃ for further use.

1.6 Synthesis of CdSe QDs-Au-GR nanocomposite

Different volumes of Au_x clusters aqueous solution (Concentration: 0.4 mg mL^{-1}; 0.5, 1, 2, 4, and 6 mL, corresponding to the weight percentages of 0.33, 0.67, 1.33, 2.67, and 4%) were added into 3 mL positively-charged EDC-modified GO (C=0.2 mg mL^{-1}) suspension under vigorous stirring for 1h. The mixture was following added into 10 mL CdSe QDs aqueous solution (C=6 mg mL^{-1}) with vigorous stirring for 1h. The precipitation was centrifuged and transferred to a 50 mL Teflon-lined stainless steel autoclave containing 15 mL of DI H_2O and 5 mL of ethanol. Hydrothermal treatment was then

conducted at 373 K for 12 h and the samples were washed with ethanol and DI H_2O and finally dried in vacuum at 313 K.

1.7 Characterization

ζ-potential measurements were performed by dynamic light-scattering analysis (ZetasizerNano ZS-90). The crystal structure was studied by X-ray di□raction (XRD, X'Pert Pro MPD, Philips, Holland) using Cu Kα as the radiation source under 40 kV and 40 mA. Morphologies of the samples were probed by field-emission scanning electron microscopy equipped with an energy-dispersive spectroscopy (FESEM, EDX, Philips XL-30, Philips, Holland). Transmission electron microscopy (TEM) and high-resolution (HR) TEM, EDX images were collected on JEOL-2010 with an accelerating voltage of 200 kV. Fourier transform infrared (FTIR) spectra were recorded on a TJ270-30A infrared spectrophotometer (Tianjin, China). X-ray photoelectron spectroscopy (XPS) spectra were recorded on a photoelectron spectrometer (ESCALAB 250, Thermo Scientific, America), for which binding energy (BE) of the elements was calibrated by the BE of carbon (284.60 eV). UV-vis di□use reflectance spectra (DRS) (Varian Cary 500 UV-vis spectrophotometer, Varian, America) were obtained using $BaSO_4$ as the reflectance background ranging from 250 to 800 nm. Brunauer-Emmett-Teller (BET) specific surface areas were determined on a Quantachrome Autosorb-1-C-TCD automated gas sorption analyzer. Photoluminescence (PL) spectra were collected on a Varian Cary Eclipse spectrometer. Raman measurement was carried out on Raman spectroscopy (Dxr-2xi, Thermo Scientific, America) with scans taken on an extended range from 0 to 3000 cm^{-1}.

1.8 Photoelectrochemical (PEC) measurements

PEC measurements were carried out on an electrochemical workstation (CHI660E workstation, CHI Shanghai, Inc.) with a conventional three-electrode configuration using Pt foil and an Ag/AgCl

electrode as the counter and reference electrodes, respectively, and 0.5 M Na_2SO_4 aqueous solution (pH=6.68) as the electrolyte. The working electrode was prepared on fluorine-doped tin oxide (FTO) glass that was cleaned by sonication in ethanol for 30 min and dried at 313 K. The boundary of FTO glass was protected using Scotch tape. Next, 5 mg of the sample was dispersed in 0.5 mL of ethanol by sonication to get a slurry which was spread onto the pretreated FTO glass. After air-drying, the Scotch tape was unstuck and the uncoated part of the electrode was isolated with nail polish. The exposed area of the working electrode was 1 cm^2. Finally, the working electrode were vertically dipped into the electrolyte and irradiated with visible light ($\lambda > 420$ nm) (PLS-SXE300D, Beijing Perfect Light Co. Ltd, China). The working electrodes were irradiated by visible light from a 300 W Xe arc lamp (PLS-SXE300D, Beijing Perfectlight Co. Ltd, China) equipped with a cutoff filter ($\lambda > 420$ nm). Potentials of the electrode were calibrated against the reversible hydrogen electrode (RHE) based on the following formula:

$$E_{RHE}=E_{Ag/AgCl}+0.059pH+E^{\circ}_{Ag/AgCl}, \text{ with } E^{\circ}_{Ag/AgCl}=0.1976V \text{ at } 25℃$$

Transient photocurrent response (i.e., *I-t*) was collected under visible light irradiation at a bias of 1.23 V vs. RHE. Electrochemical impedance spectra (EIS) were measured on an IM6 electrochemical station (Interface 1000E, Gamry, American) with an amplitude of 10 mV in the frequency range of 105 kHz to 0.1 Hz in a $K_3[Fe(CN)_6]$ aqueous solution (5 mM, pH=7).

1.9 Selective Photoreduction performances

Selective photocatalytic reduction of nitroaromatics to the corresponding amides was carried out as follows: 10 mg of catalyst and 40 mg of Na_2SO_3 were added into 30 mL of nitroaromatics aqueous solution (5 ppm), which is saturated with N_2 bubbling at ambient conditions. After vigorously stirring in dark for 1 h to reach the adsorption-desorption equilibrium, the glass vessel was irradiated by visible

light ($\lambda > 420$ nm). Then, 3 mL of the solution was taken out at a given time interval (2 min) and centrifuged at 12000 rpm for 10 min to completely remove the catalysts and the supernatant was analyzed by a Varian Cary 50 UV-vis spectrophotometer. Photoactivity of the sample was defined by the following formula,

$$\text{Conversion (\%)} = \frac{C_0 - C}{C_0} \times 100\%$$

where C_0 represents the initial concentration of nitroaromatics and C is the concentration after a certain time visible light irradiation.

2. Supporting data

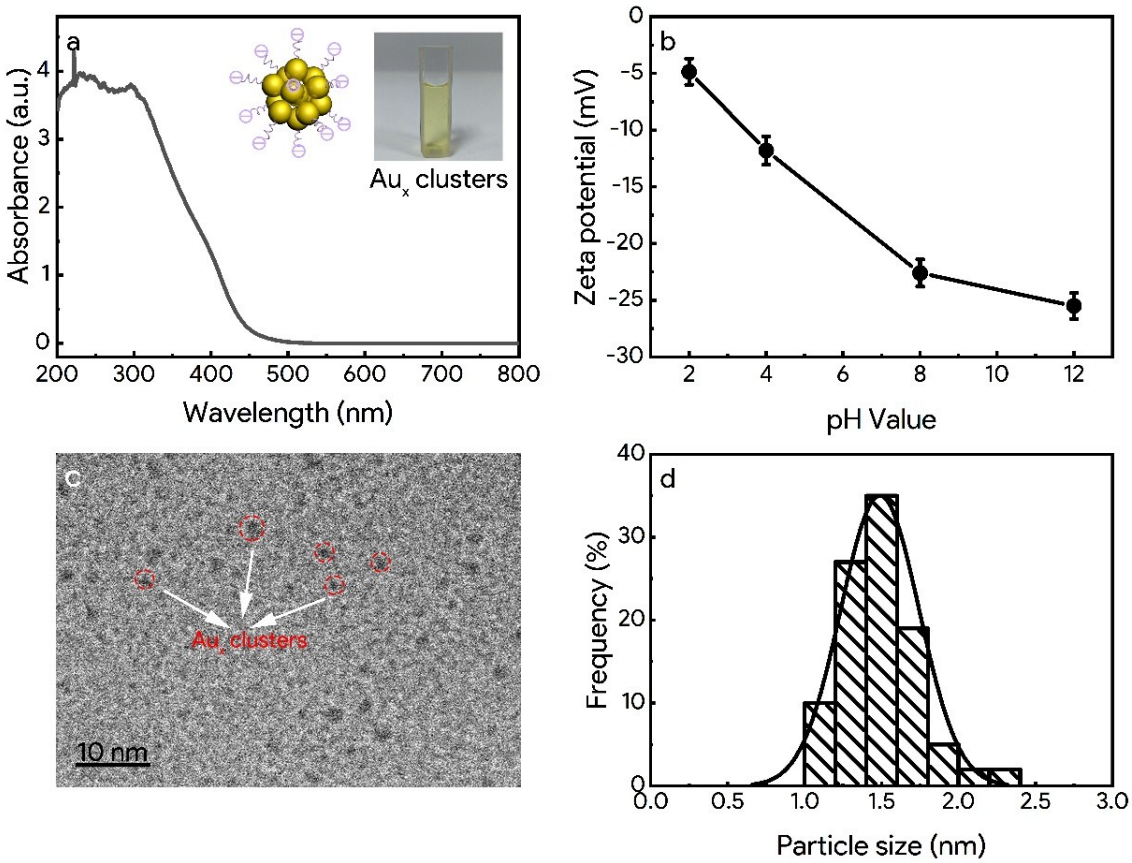

Fig. S1. (a) UV-vis adsorption spectrum with photograph and schematic model in the inset, (b) zeta potential, (c) TEM image with corresponding (d) size distribution histogram of GSH-capped Au_x clusters.

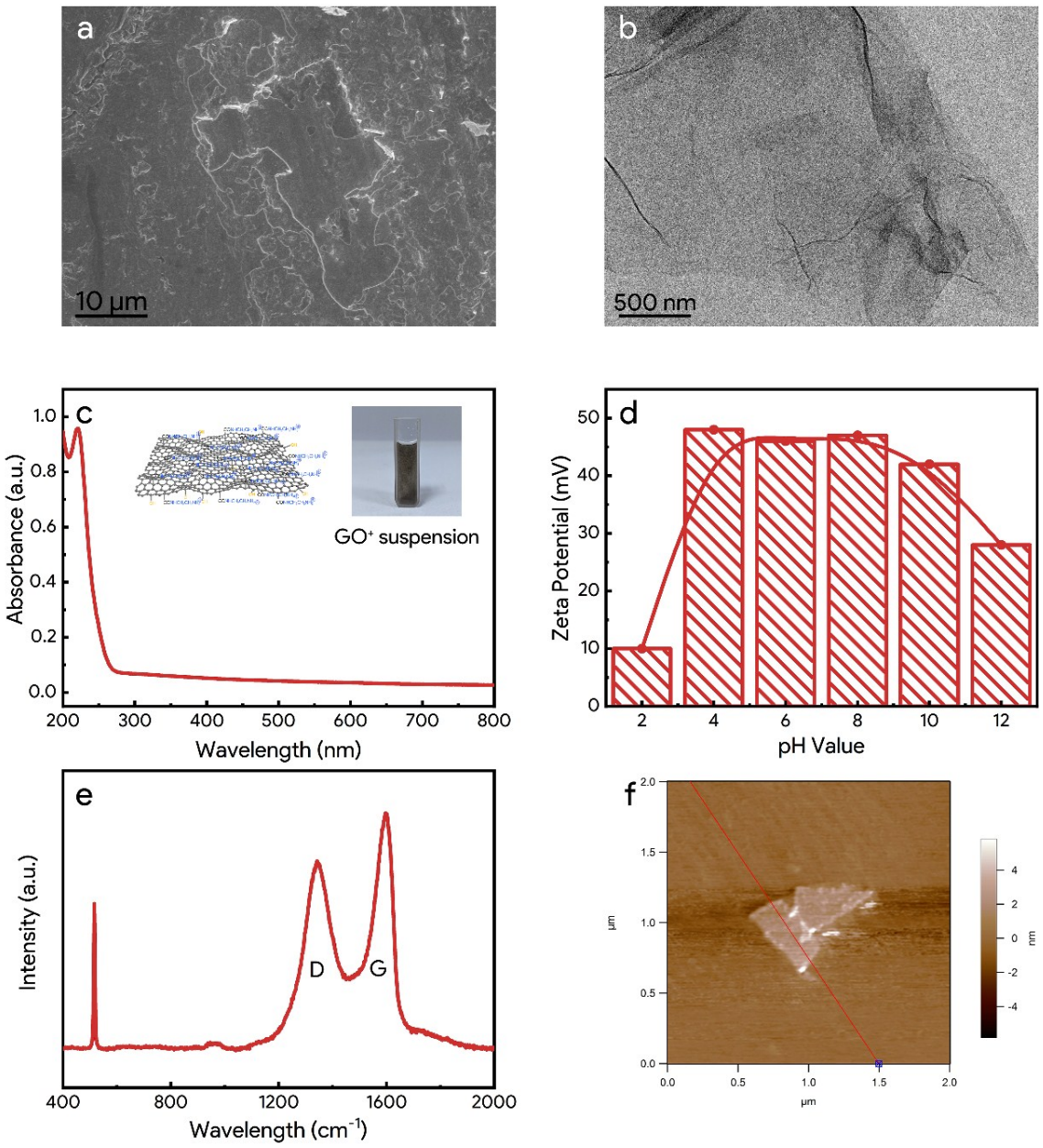

Fig. S2. (a) FESEM, (b) TEM images, (c) UV-vis absorption spectrum with graph in the inset, (d) zeta potentials, (e) Raman spectrum, and (f) AFM image of EDC-modified positively charged GO (GO^+).

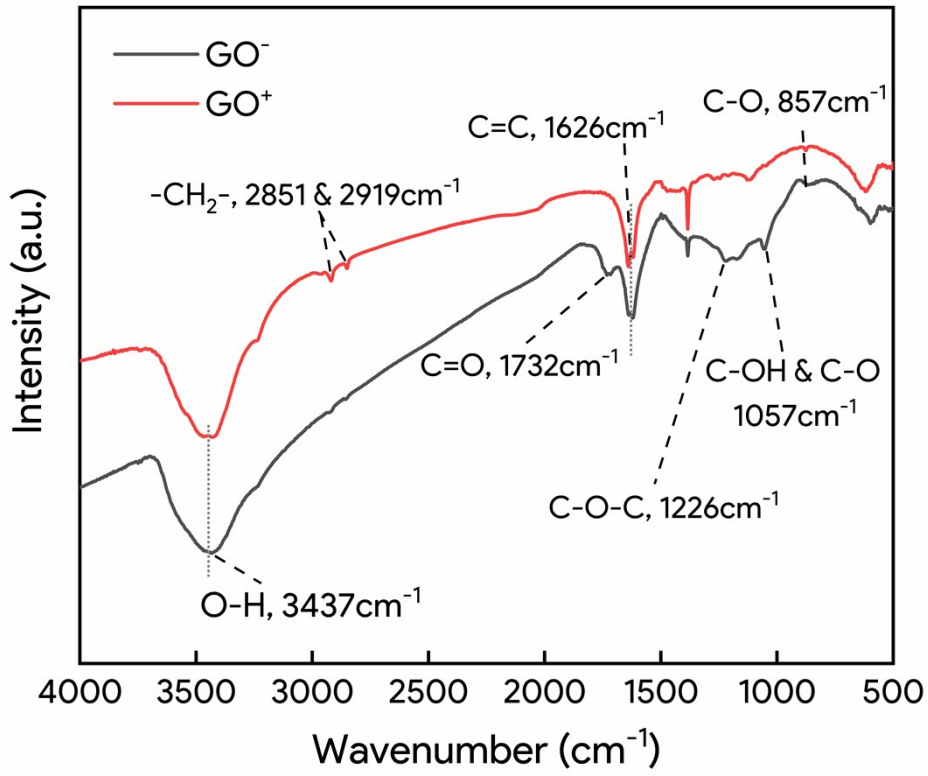

Fig. S3. FTIR spectra of negatively charged GO (GO^-) and positively charged GO (GO^+) nanosheets.

Note: The peaks at ca. 3437, 1732, 1057 & 857, 1626, and 1226 cm^{-1} in the FTIR spectrum of GO^- are ascribed to the hydroxyl groups (-OH), carboxyl groups (C=O), alkoxy groups (C-OH & C-O), aromatic C=C bonds, and epoxy groups (C-O-C), respectively. With regard to the FTIR spectrum of EDC-modified GO (GO^+) which shows two characteristic peaks at 2851 and 2919 cm^{-1}, attributable to the methylene groups ($-CH_2-$) from ethylenediamine, corroborating anchoring of EDC on the GO^+ framework. Noteworthily, C=O stretching vibration peak at 1732 cm^{-1} was not observed in the FTIR spectrum of GO^+, indicating partial reduction of GO^+ to GR.

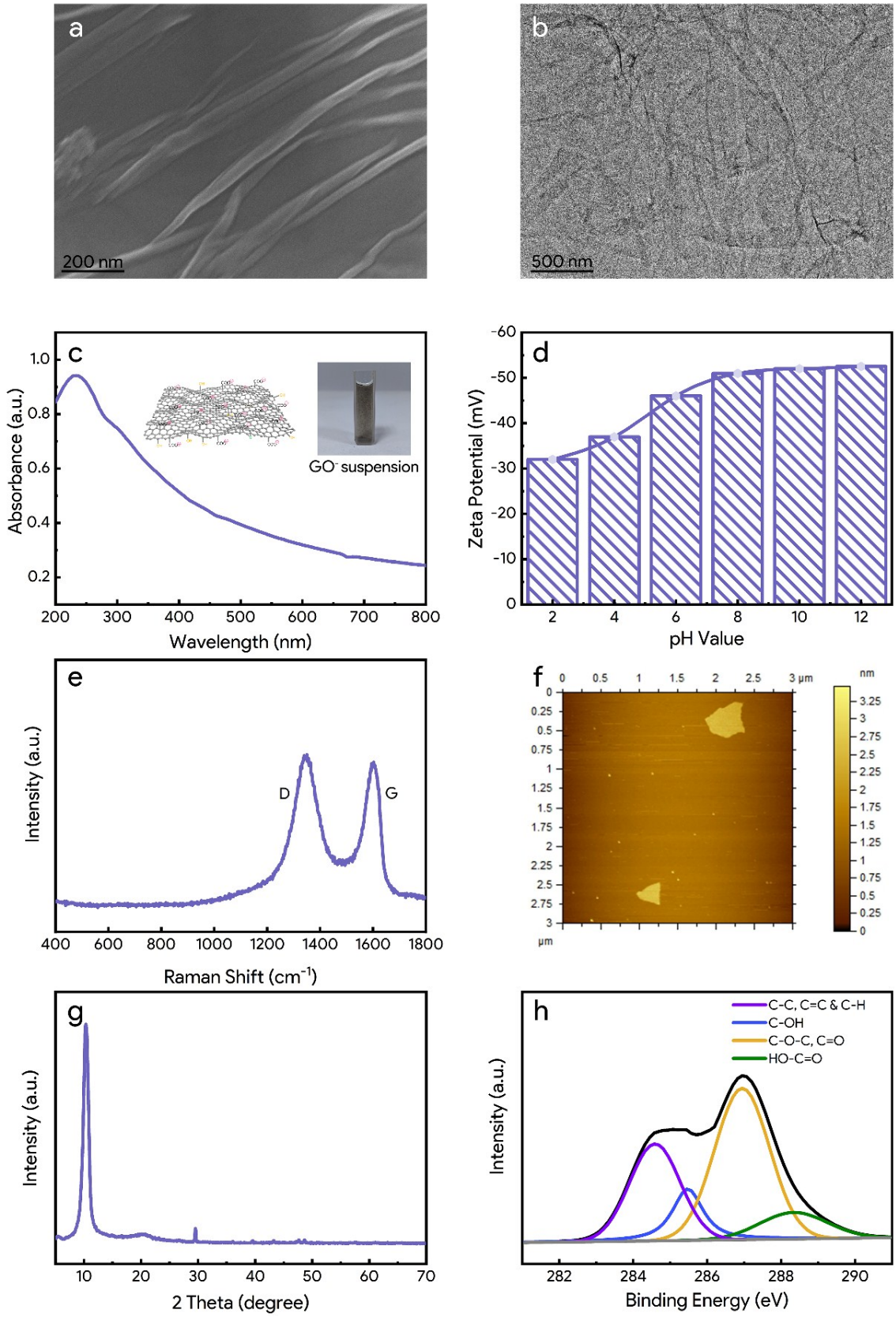

Fig. S4. (a) FESEM, (b) TEM, (c) UV-vis absorption spectrum with graph in the inset, (d) zeta potential, (e) Raman spectrum, (f) AFM image, (g) XRD pattern, and high-resolution C 1s spectra (h) of pristine negatively charged GO^- precursor.

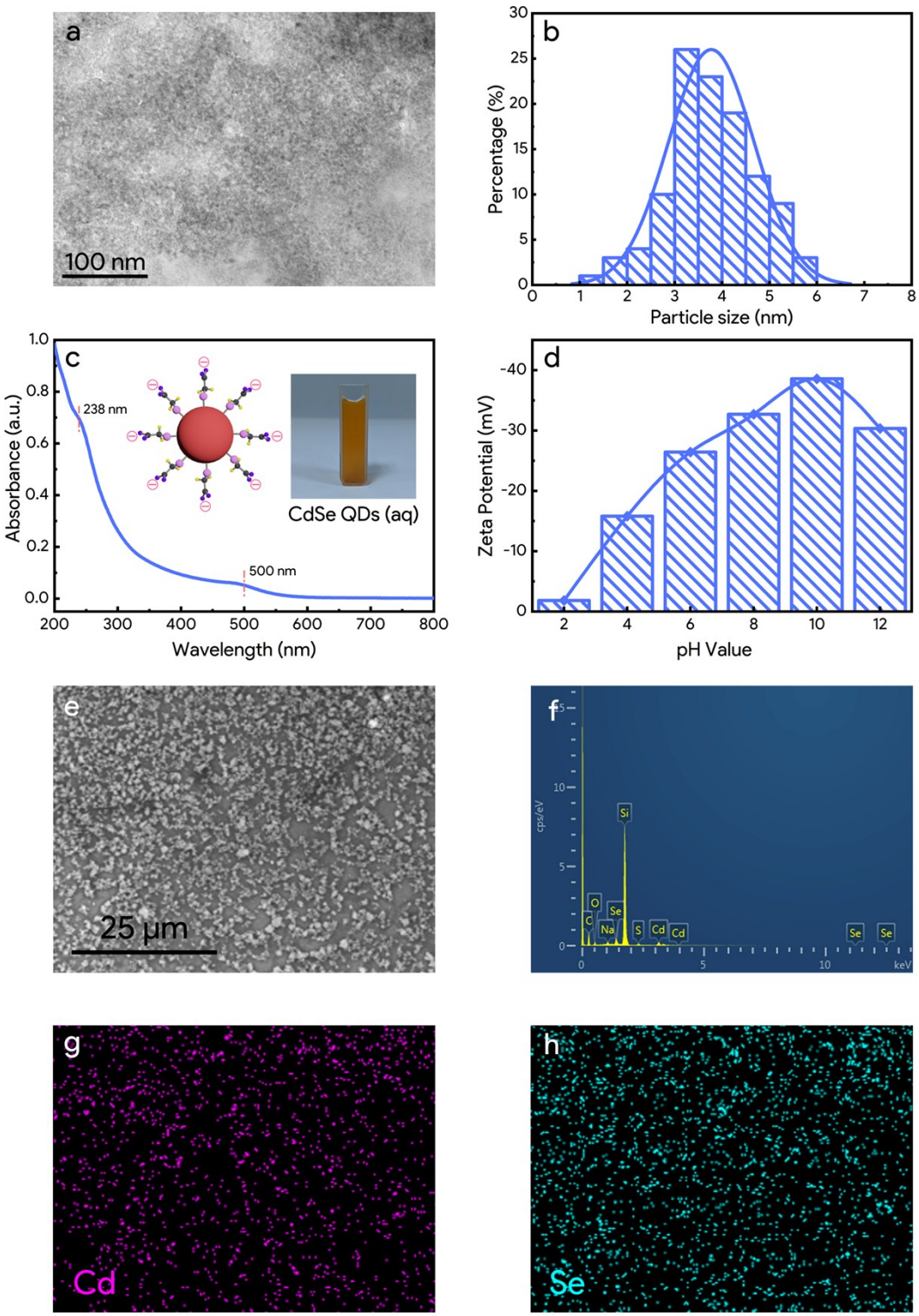

Fig. S5. (a) TEM image with corresponding (b) size distribution histogram, (c) UV-vis absorption spectrum with graph and schematic model in the inset, (d) zeta potentials, (e) FESEM image with the corresponding (f) EDX, and (g−h) elemental mapping results of CdSe QDs@MAA.

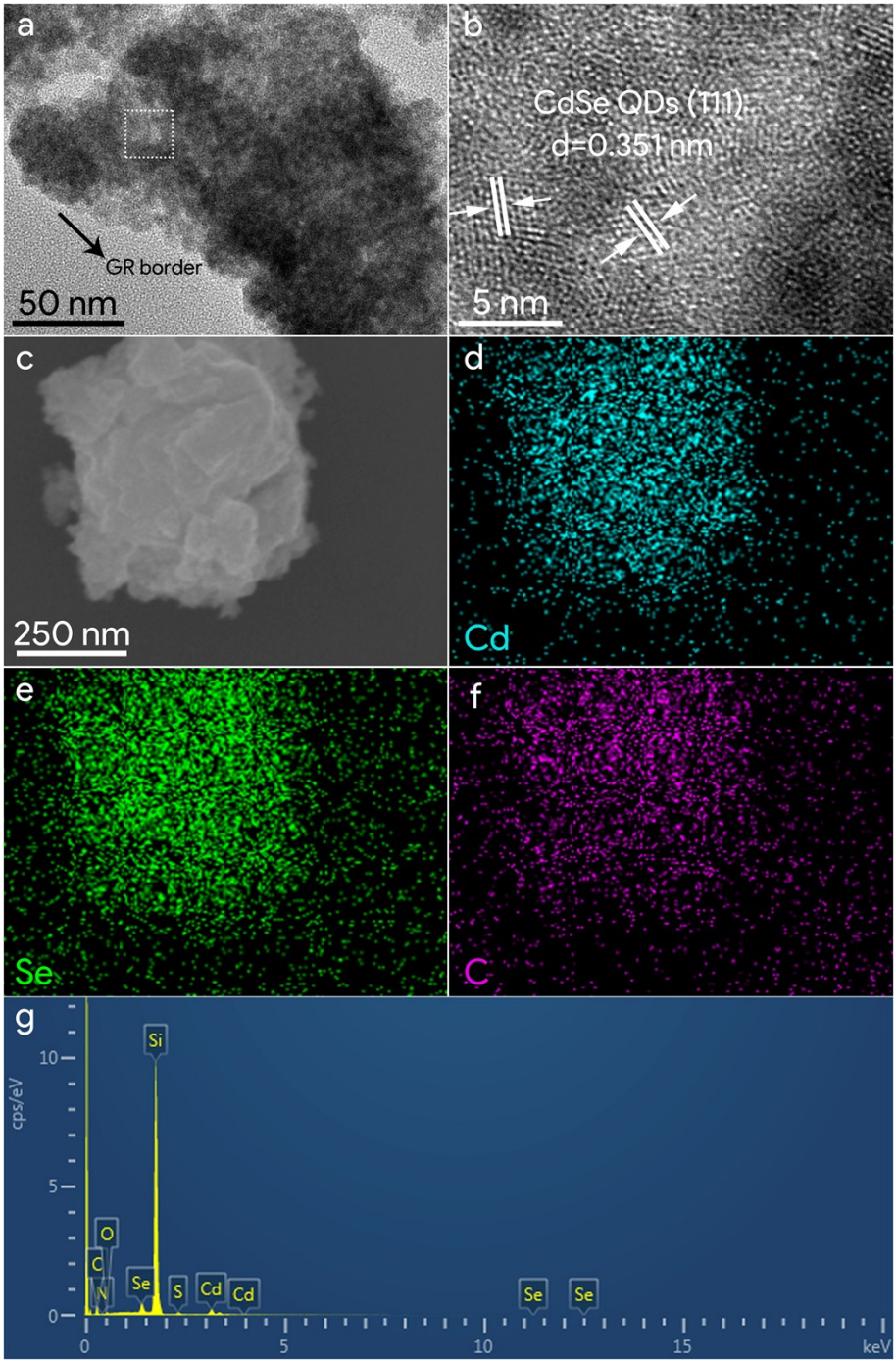

Fig. S6. (a) TEM and (b) HRTEM, (c) FESEM images with corresponding (d−f) elemental mapping and (g) EDX results of CdSe QDs-GR nanocomposites.

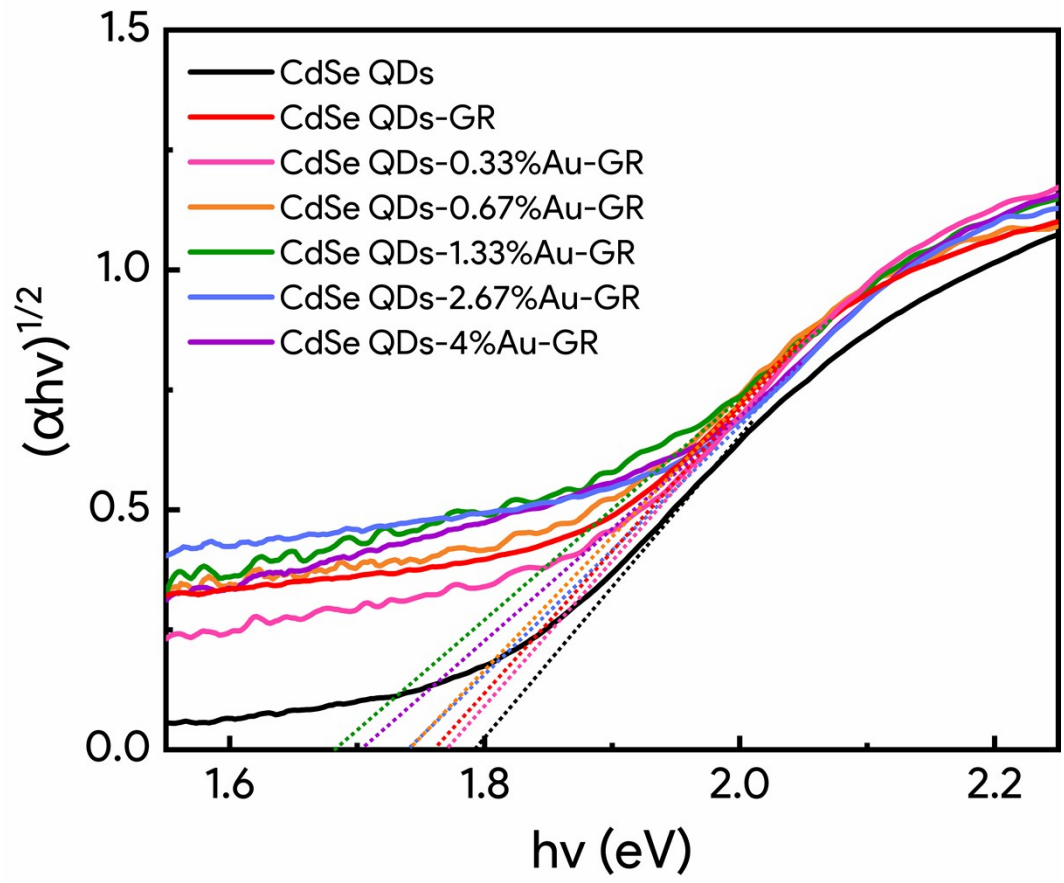

Fig. S7. The transformed plots based on the Kubelka-Munk function vs. photon energy for CdSe QDs-Au-GR nanocomposites with different loading percentage of Au NPs and the loading percentage of GR was controlled to be 1.0 %.

Note: Bandgaps (E_g) of these samples are roughly estimated to be ca. 1.77, 1.74, 1.68, 1.74, and 1.70 eV, corresponding to the CdSe QDs-Au-GR nanocomposites with Au loading percentage of 0.33, 0.67, 1.33, 2.67, and 4 %, respectively.

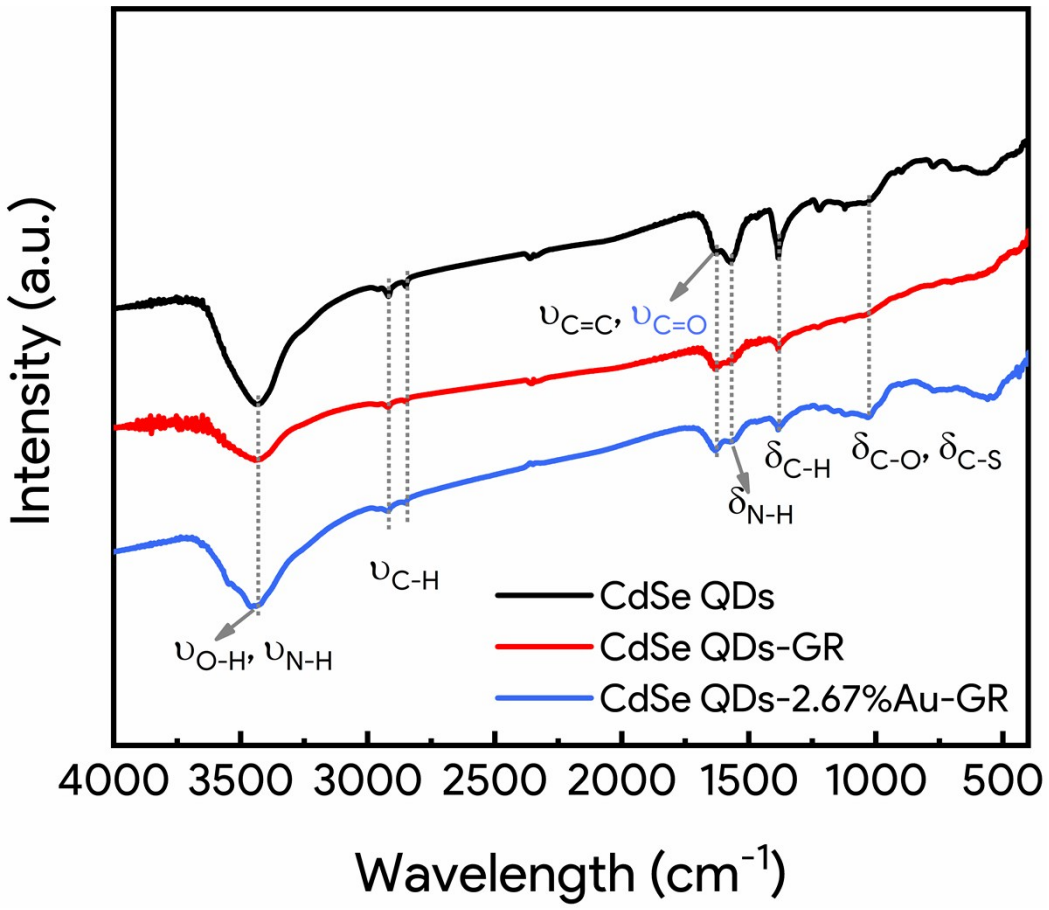

Fig. S8. FTIR spectra of blank CdSe QDs, CdSe QDs-GR, and CdSe QDs-2.67%Au-GR nanocomposite.

Table S1. Functional groups vs. wavenumber for different samples

Wavenumber (cm^{-1})	*Vibrational mode*	*Functional groups & Ingredient*
3433	υ_{O-H} & υ_{N-H}	-COOH & -NH_2/MAA & GO^+
2918 & 2850	υ_{C-H}	-CH_2-/MAA & GSH
1632	$\upsilon_{C=C}$ & $\upsilon_{C=O}$	C=C & C=O/GR
1574	δ_{N-H}	-NH_2/GO^+
1385	δ_{C-H}	-CH_2- & -CH_3
1090	δ_{C-O} & δ_{C-S}	GSH

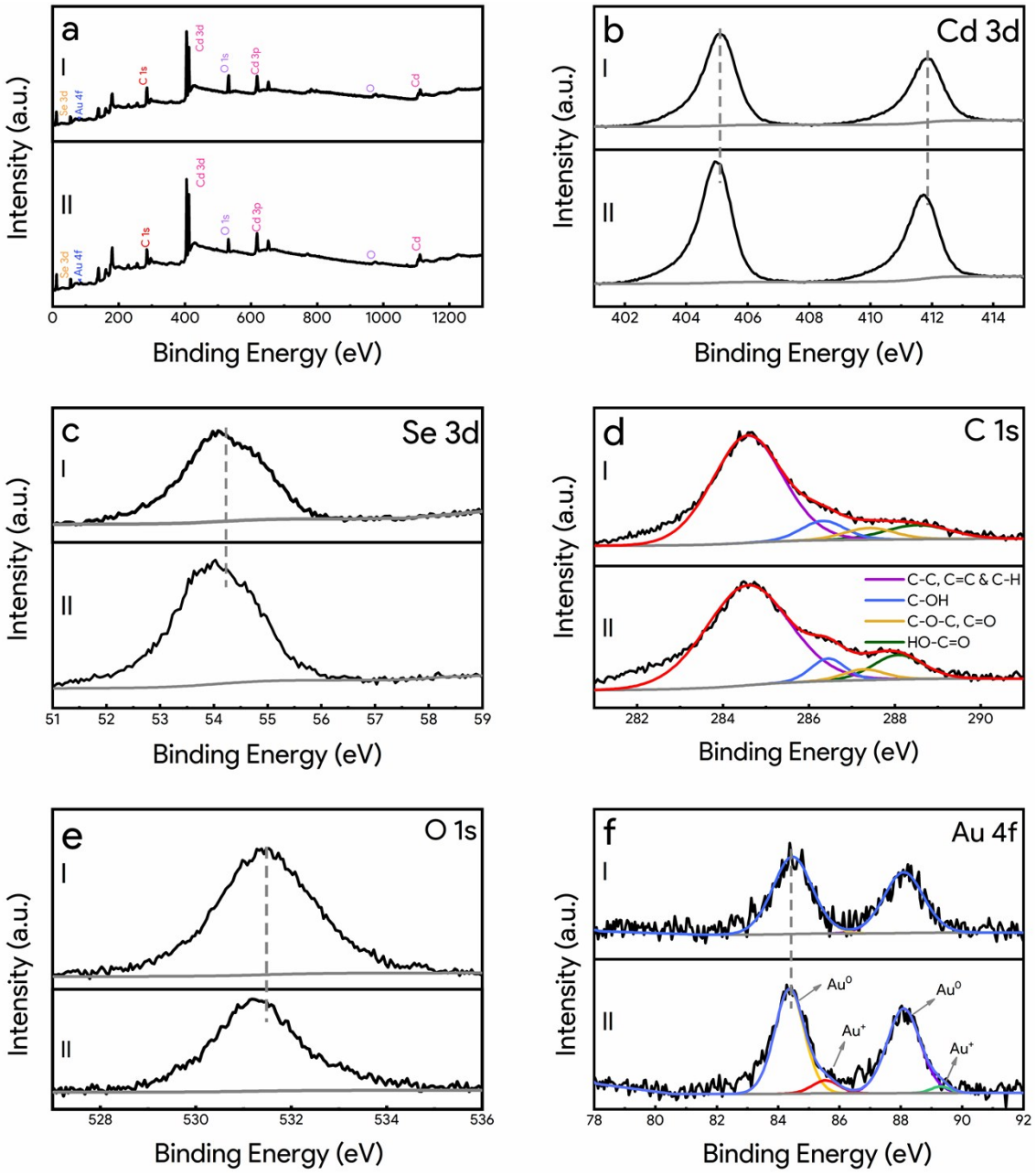

Fig. S9. Survey spectra and high-resolution (b) Cd 3d, (c) Se 3d, (d) C 1s, (e) O 1s, and (f) Au 4f spectra of (I) CdSe QDs-2.67%Au-GR and (II) CdSe QDs-2.67%Au_x-GR nanocomposite.

Table S2. Chemical bond species vs. B.E. for different samples

Element	***CdSe QDs-2.67%Au-GR***	***CdSe QDs-2.67%Au_x-GR***	***Chemical Bond Species***
Cd $3d_{3/2}$	411.85 eV	411.55 eV	Cd^{2+}
Cd $3d_{5/2}$	405.09 eV	404.8 eV	Cd^{2+}
Se 3d	54.23 eV	53.85 eV	Se^{2-}
C 1s	284.60 eV	284.60 eV	C-C, C=C & C-H
	286.65 eV	286.75 eV	C-OH
	287.74 eV	287.40 eV	C-O-C, C=O
	288.55 eV	288.10 eV	HO-C=O
O 1s	531.47 eV	531.07 eV	O^{2-}
Au $4f_{5/2}$	88.11 eV	87.92 eV	Metallic Au^0
Au $4f_{7/2}$	84.49 eV	84.19 eV	Metallic Au^0
Au $4f_{5/2}$	*Not detected*	89.12 eV	Au^+
Au $4f_{7/2}$	*Not detected*	85.37 eV	Au^+

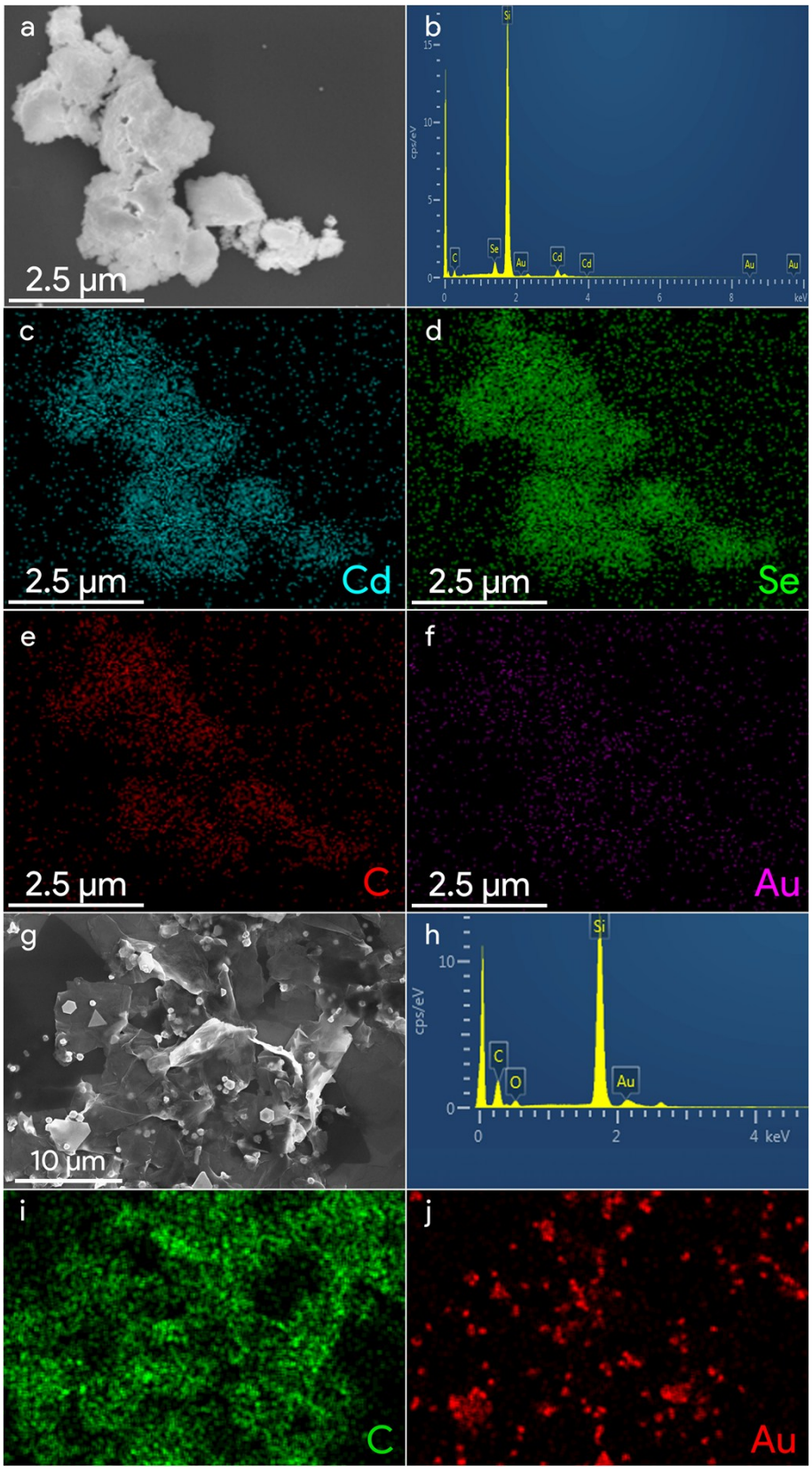

Fig. S10. (a) FESEM image with corresponding (d) EDX and (b, c, e, f) elemental mapping results of CdSe QDs-2.67%Au-GR nanocomposite; (g) FESEM images with corresponding (h) EDX and (i–j) elemental mapping results of 2.67%Au-GR nanocomposite.

Note: FESEM elemental mapping results along with the TEM elemental mapping results (**Fig. 2)** demonstrate clear signals of Cd, Se, and C elements with apparent border and shape, as displayed in **Fig. S10** (**c-e**). Notably, **Fig. S10 (b & f)** shows negligible Au signal and this is understandable in terms of electrostatic self-assembly of Au NCs in the interfacial domain of CdSe QDs and GR rather than on the surface. Additionally, Au NPs-GR binary nanocomposite with the same weight ratio was prepared and its morphology was displayed in **Fig. S10 (g-j)**. Clear distribution pattern of Au signal in the Au NPs-GR was determined by the elemental mapping result (**Fig. S10j**), once again corroborating our speculation that Au NPs signal in the elemental mapping result of CdSe QDs-2.67%Au-GR was shielded by CdSe QDs encapsulation. This deduction can be strongly corroborated by the elemental mapping results from HRTEM measurements in **Fig. 2g**.

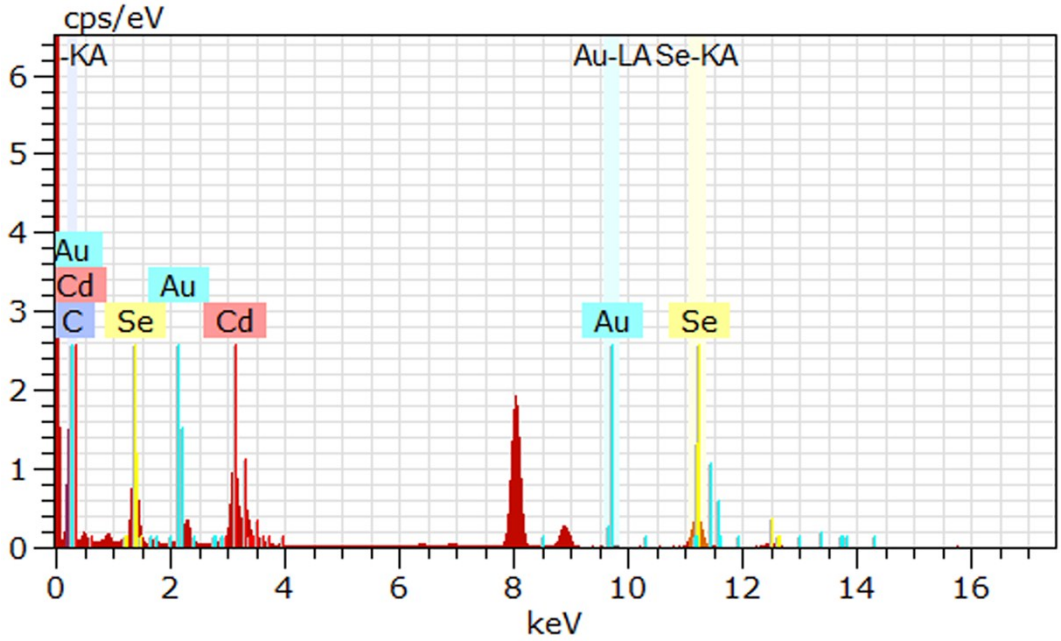

Fig. S11. HRTEM-EDX result of CdSe QDs-2.67%Au-GR nanocomposite.

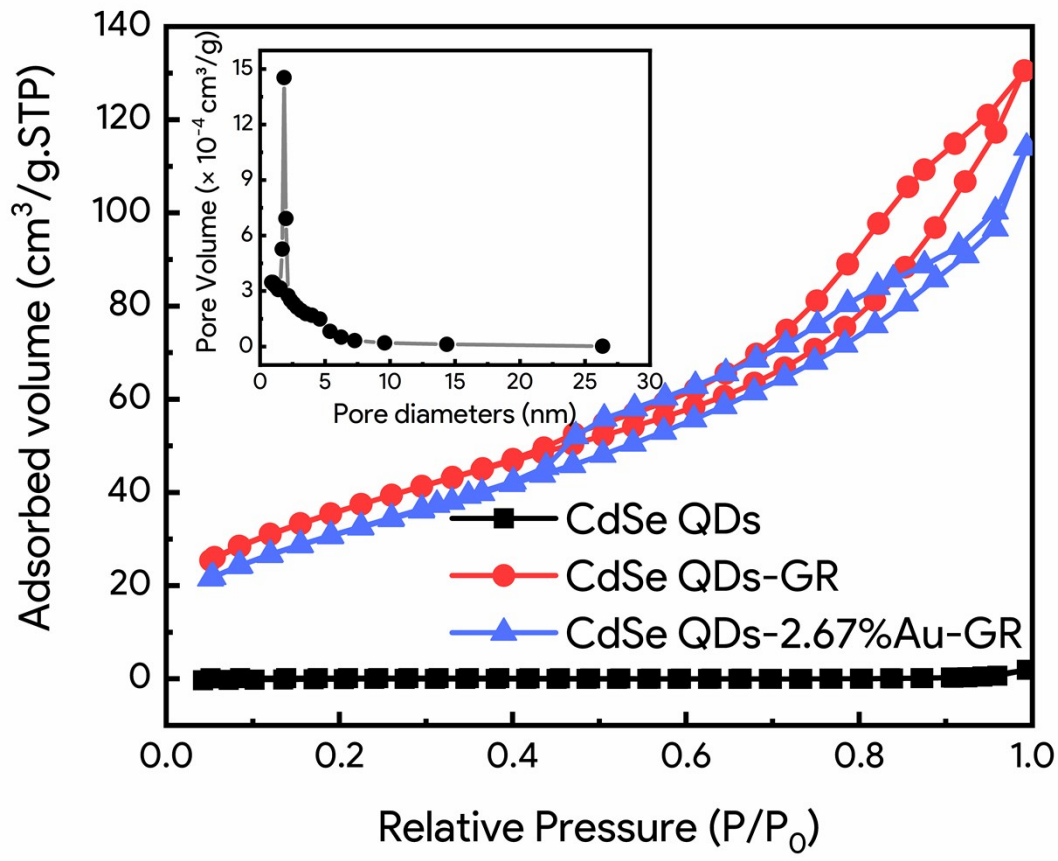

Fig. S12. N_2 adsorption-desorption isotherms of blank CdSe QDs, CdSe QDs-GR, and CdSe QDs-2.67%Au-GR nanocomposite with pore size distribution of CdSe QDs-2.67%Au-GR nanocomposite in the inset.

Table S3. Specific surface areas and pore size for different samples.

Sample	CdSe QDs	CdSe QDs-GR	CdSe QDs-2.67%Au-GR
S_{BET} (m^2 g^{-1})	0.48	131.48	115.89
Pore size (nm)	5.10	5.38	5.02

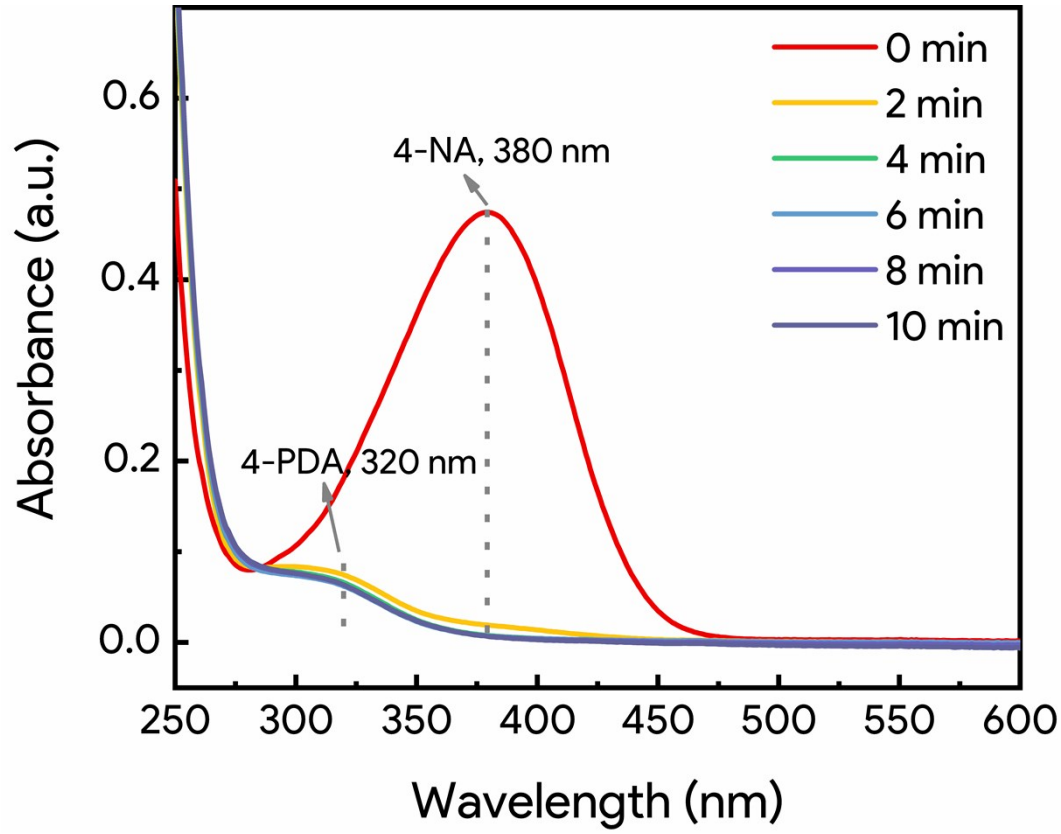

Fig. S13. UV-vis absorption spectra of 4-NA under visible light (λ>420nm) irradiation in the presence of CdSe QDs-2.67%Au-GR nanocomposite.

Note: Time-online UV-vis absorption spectra of 4-NA were used to probe the conversion of 4-NA to 4-PDA. As exhibited in **Fig. S13**, absorption peak intensity of 4-NA at 380 nm gradually decreases with prolonging the irradiation time and meanwhile the absorption peak of 4-PDA at 320 nm appeared, indicating the conversion of 4-NA to 4-PDA under visible light irradiation.

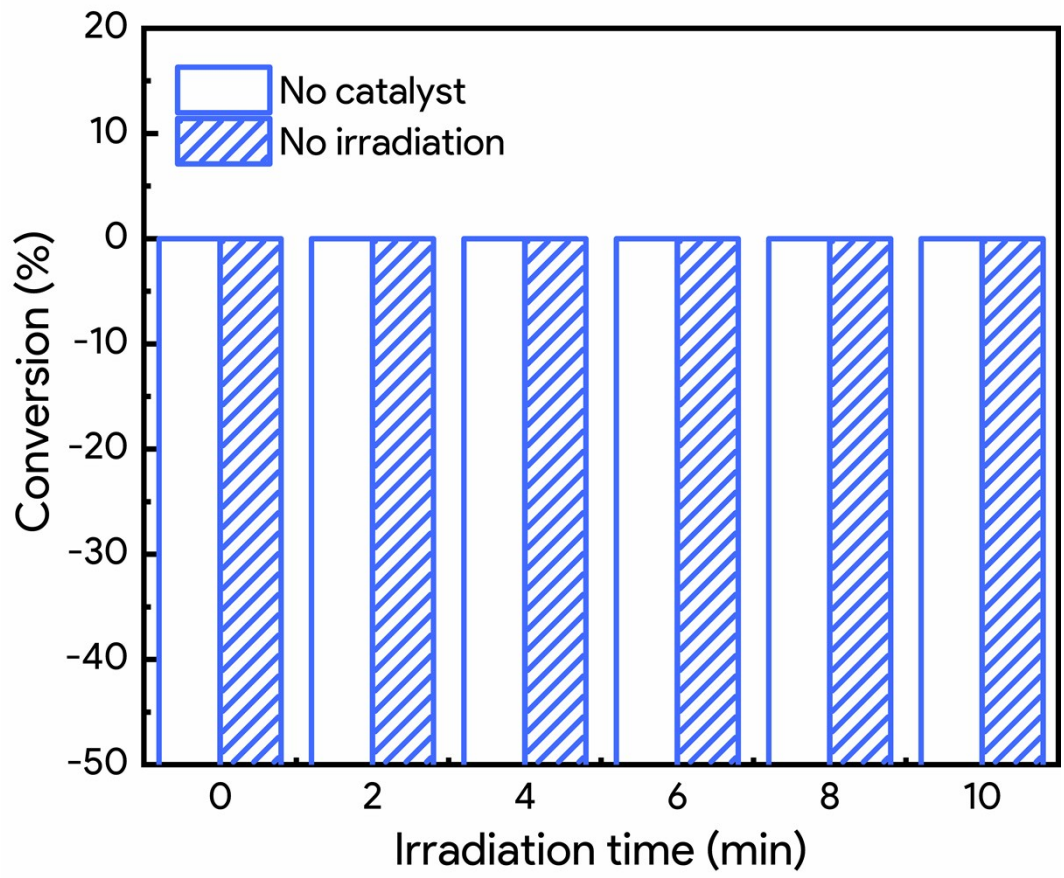

Fig. S14. Control experiments of CdSe QDs-2.67%Au-GR nanocomposite toward photoreduction of 4-NA without adding catalyst or light irradiation.

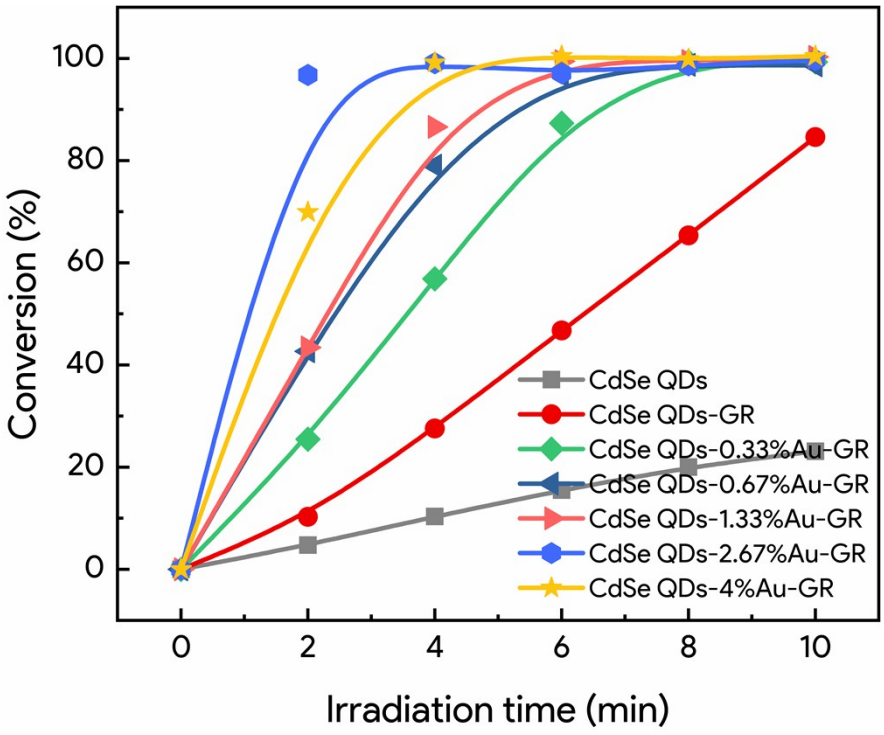

Fig. S15. Photoactivities of blank CdSe QDs, CdSe QDs-GR, and CdSe QDs-Au-GR nanocomposites with different loading percentage of Au NPs under visible light irradiation (λ>420nm) with the addition of Na_2SO_3 for quenching photogenerated holes and N_2 bubbling at ambient conditions toward 4-NA reduction.

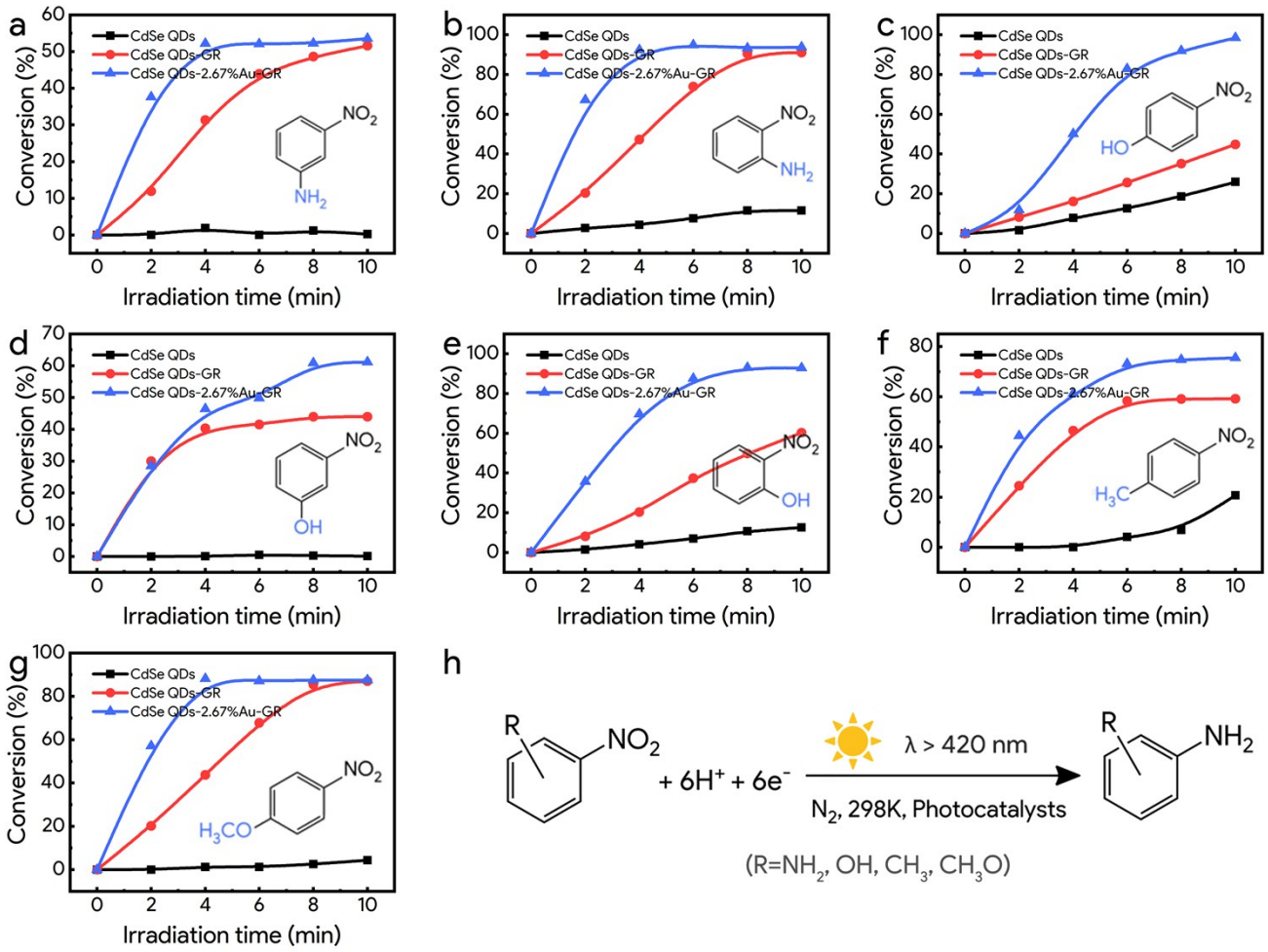

Fig. S16. Photocatalytic performances of blank CdSe QDs, CdSe QDs-GR, and CdSe QDs-2.67%Au-GR nanocomposite toward selective reduction of nitroaromatics including (a) 3-NA, (b) 2-NA, (c) 4-NP, (d) 3-NP, (e) 2-NP, (f) 4-nitrotoluene, and (g) 4-nitroanisole under visible light irradiation (λ>420 nm) with the addition of Na_2SO_3 for quenching photogenerated holes and N_2 bubbling at ambient conditions together with the (h) typical reaction model under the current experimental conditions.

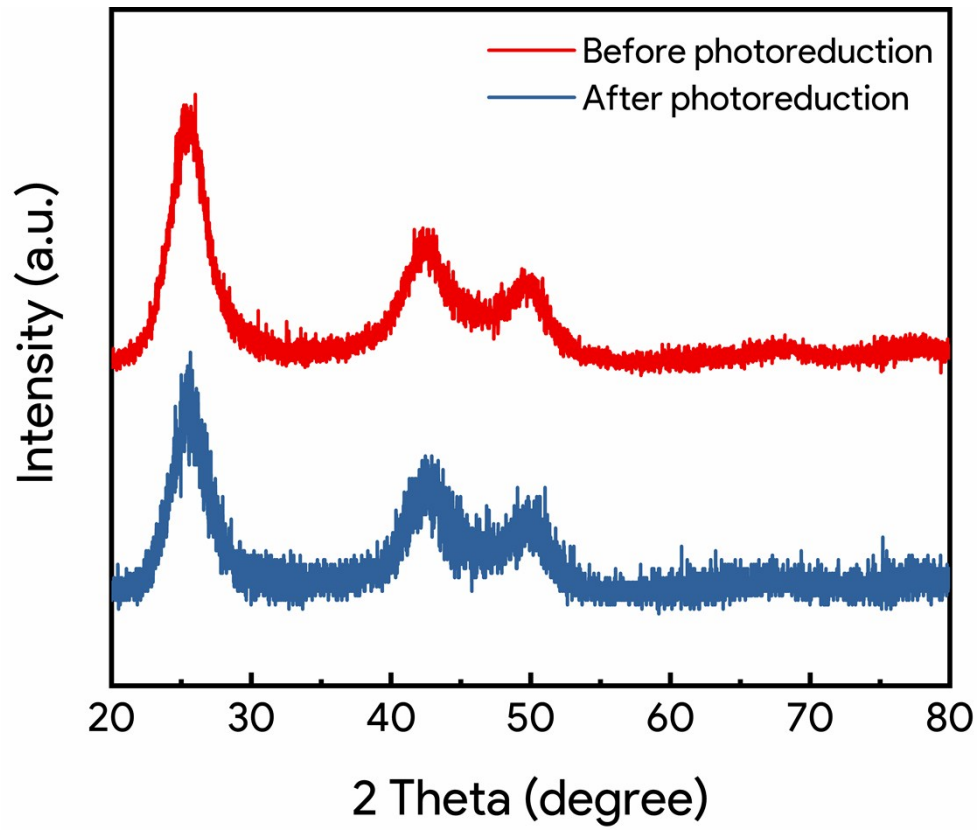

Fig. S17. XRD patterns of CdSe QDs-2.67%Au-GR nanocomposite before and after photoreduction.

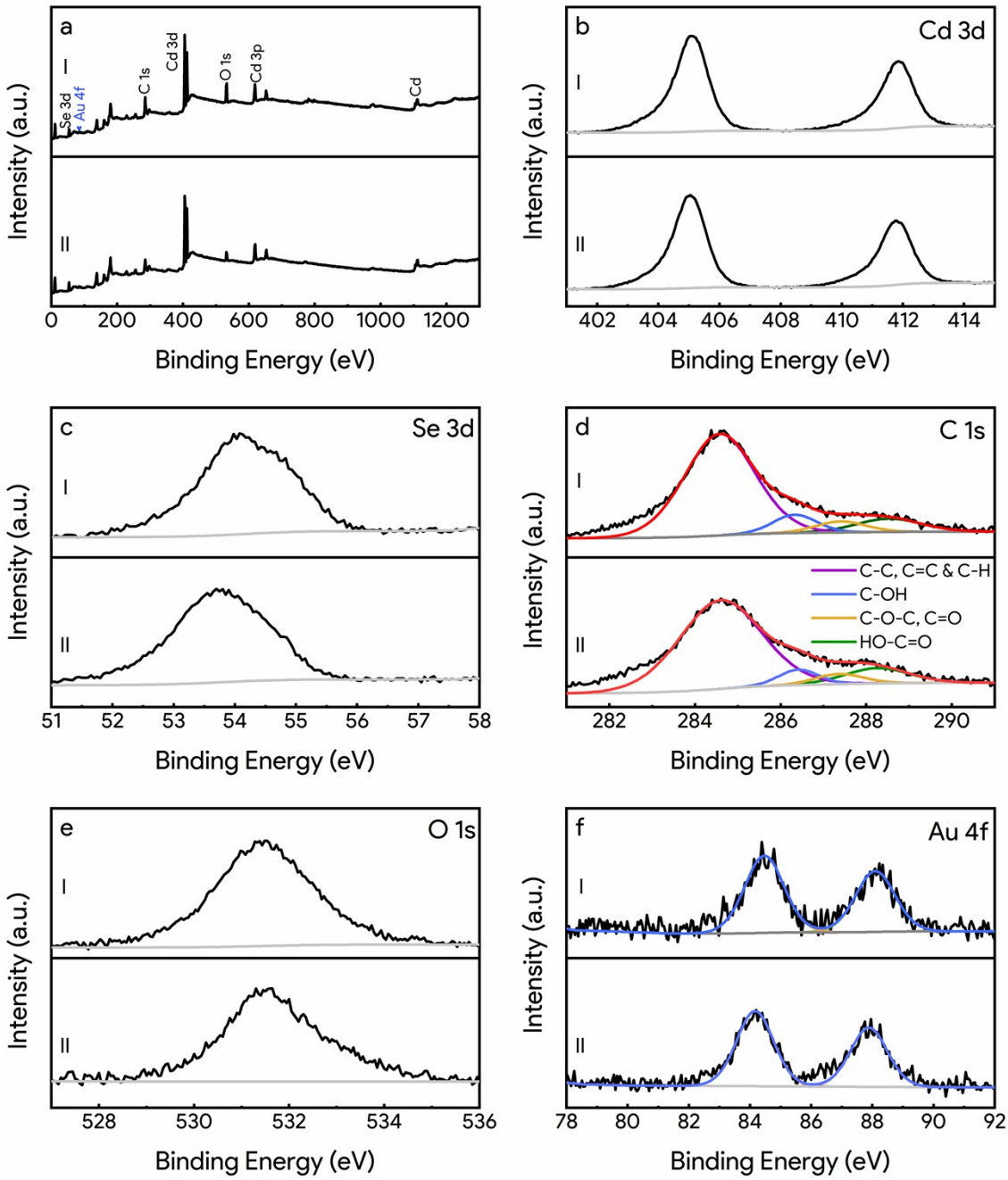

Fig. S18. Survey and high-resolution Cd 3d, Se 3d, C 1s, O 1s spectra of CdSe QDs-2.67%Au-GR nanocomposite (I) before and (II) after photoreduction reaction.

Table. S4. Chemical bond species vs. B.E. for CdSe QDs-2.67%Au-GR nanocomposite before and after photoreduction

Element	***Original***	***After reaction***	***Chemical Bond Species***
Cd $3d_{3/2}$	411.85 eV	411.80 eV	Cd^{2+}
Cd $3d_{5/2}$	405.09 eV	405.05 eV	Cd^{2+}
Se 3d	54.23 eV	53.71 eV	Se^{2-}
C 1s	284.60 eV	284.60 eV	C-C, C=C & C-H
	286.65 eV	286.65 eV	C-OH
	287.74 eV	287.37 eV	C-O-C, C=O
	288.55 eV	288.15 eV	HO-C=O
O 1s	531.47 eV	531.49 eV	O^{2-}
Au $4f_{5/2}$	88.20 eV	88.25 eV	Metallic Au^0
Au $4f_{7/2}$	84.55 eV	84.25 eV	Metallic Au^0

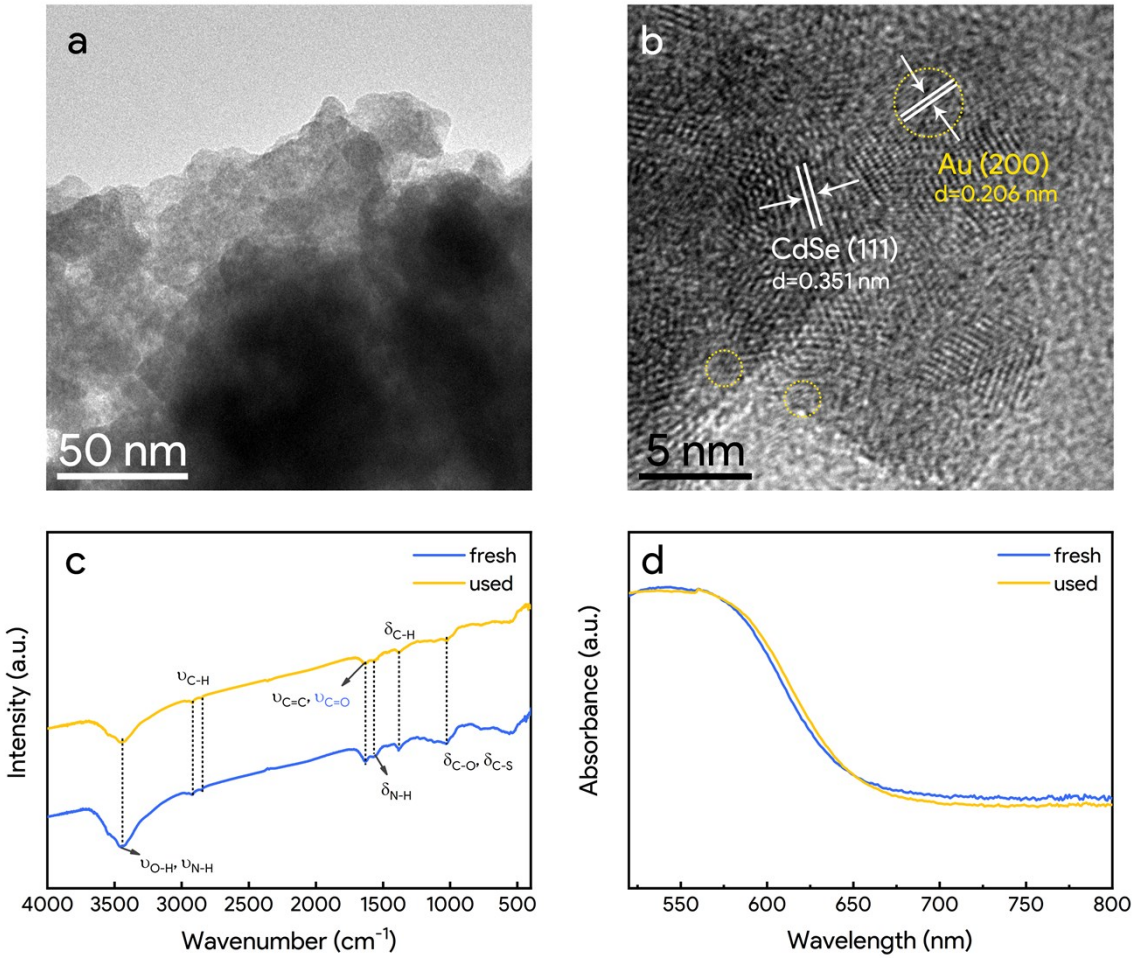

Fig. S19. Structural characterizations of CdSe QDs-2.67%Au-GR nanocomposite before and after cyclic photocatalytic reaction toward 4-NA reduction under visible light irradiation including (a) low-magnified TEM & (b) HRTEM images, (c) FTIR spectra, and (d) DRS spectra.

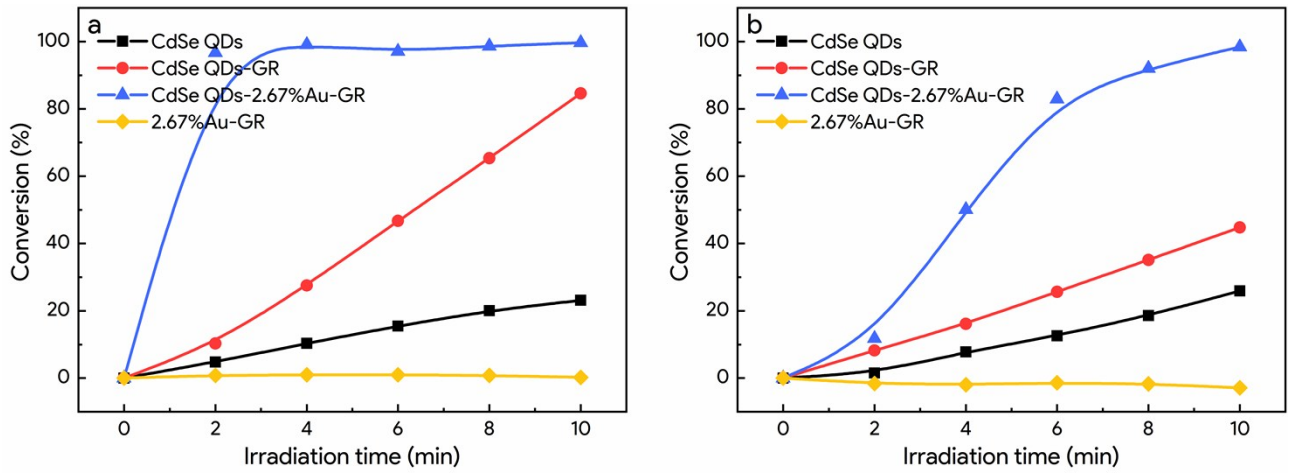

Fig. S20. Photocatalytic performances of blank CdSe QDs, CdSe QDs-GR, 2.67%Au-GR, and CdSe QDs-2.67%Au-GR nanocomposite toward selective reduction of nitroaromatics including (a) 4-NA and (b) 4-NP under visible light irradiation (λ>420 nm) with the addition of Na_2SO_3 for quenching photogenerated holes and N_2 bubbling at ambient conditions.

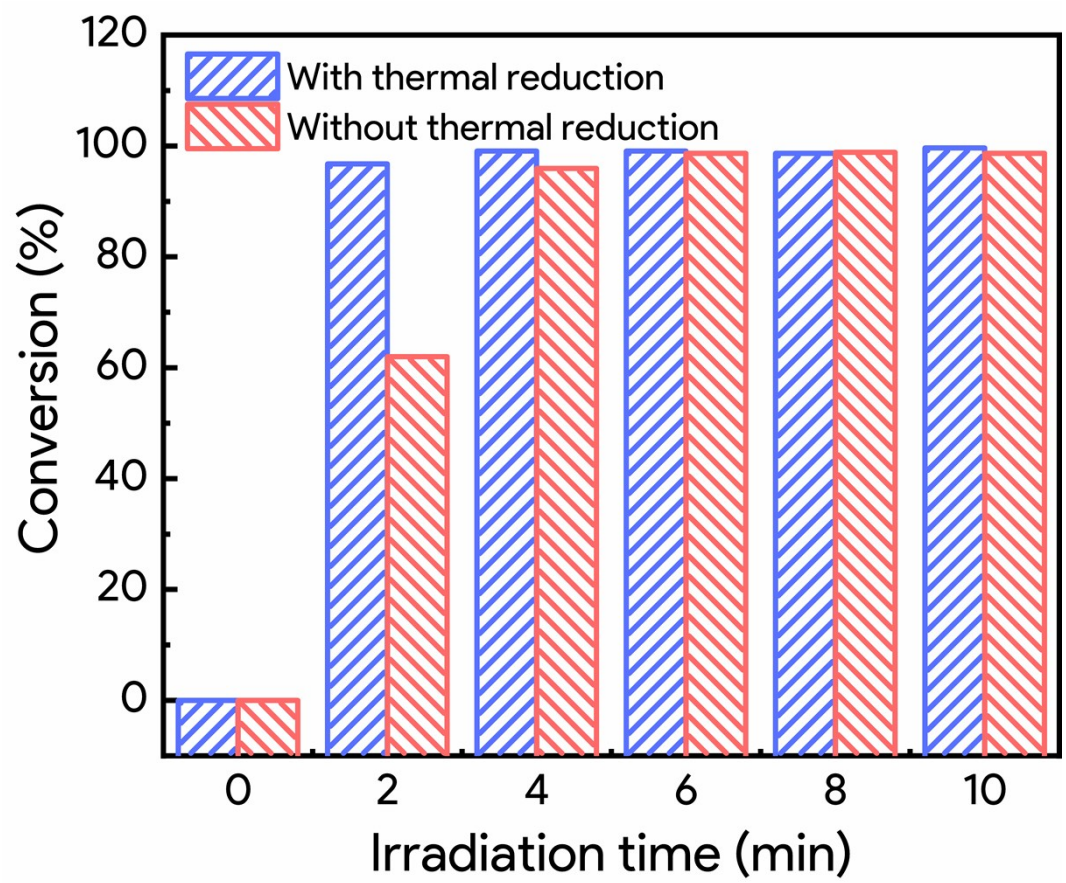

Fig. S21. Control experiments of CdSe QDs-2.67%Au-GR nanocomposite toward photoreduction of 4-NA with and without thermal reduction.

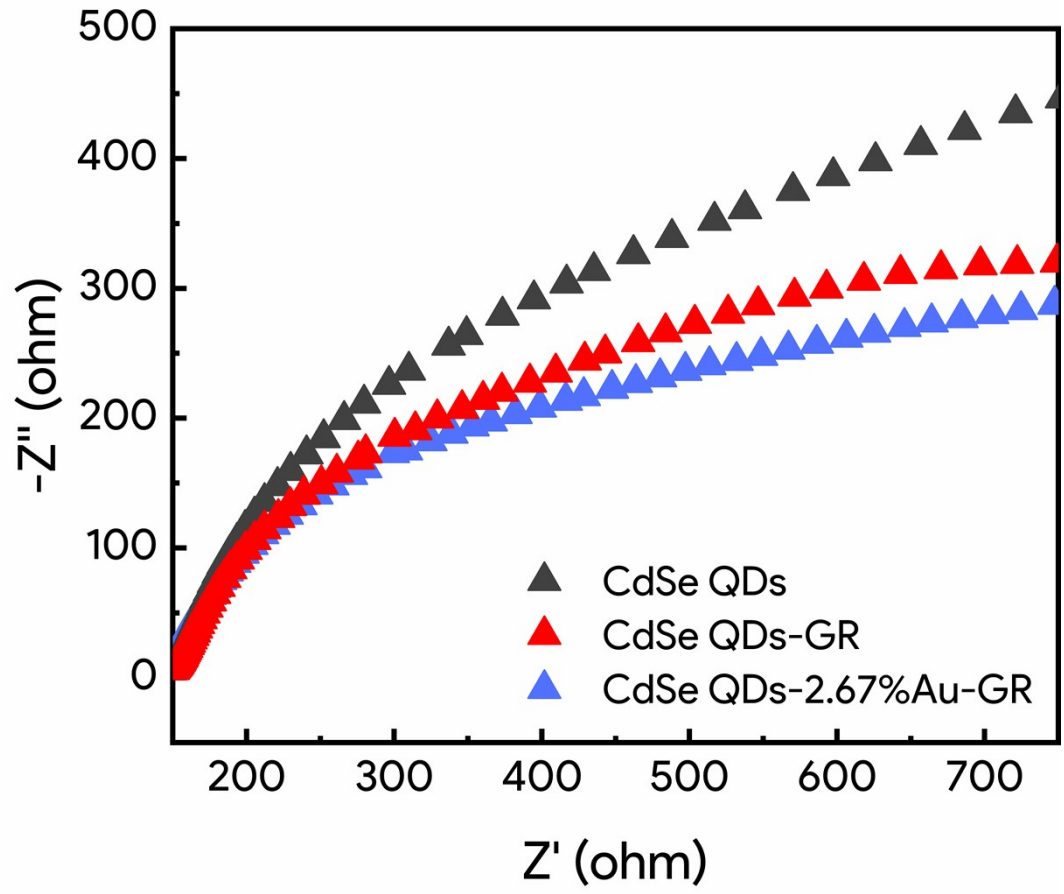

Fig. S22. EIS Nyquist plots of blank CdSe QDs, CdSe QDs-GR, and CdSe QDs-2.67%Au-GR nanocomposite under visible light irradiation (λ>420 nm).

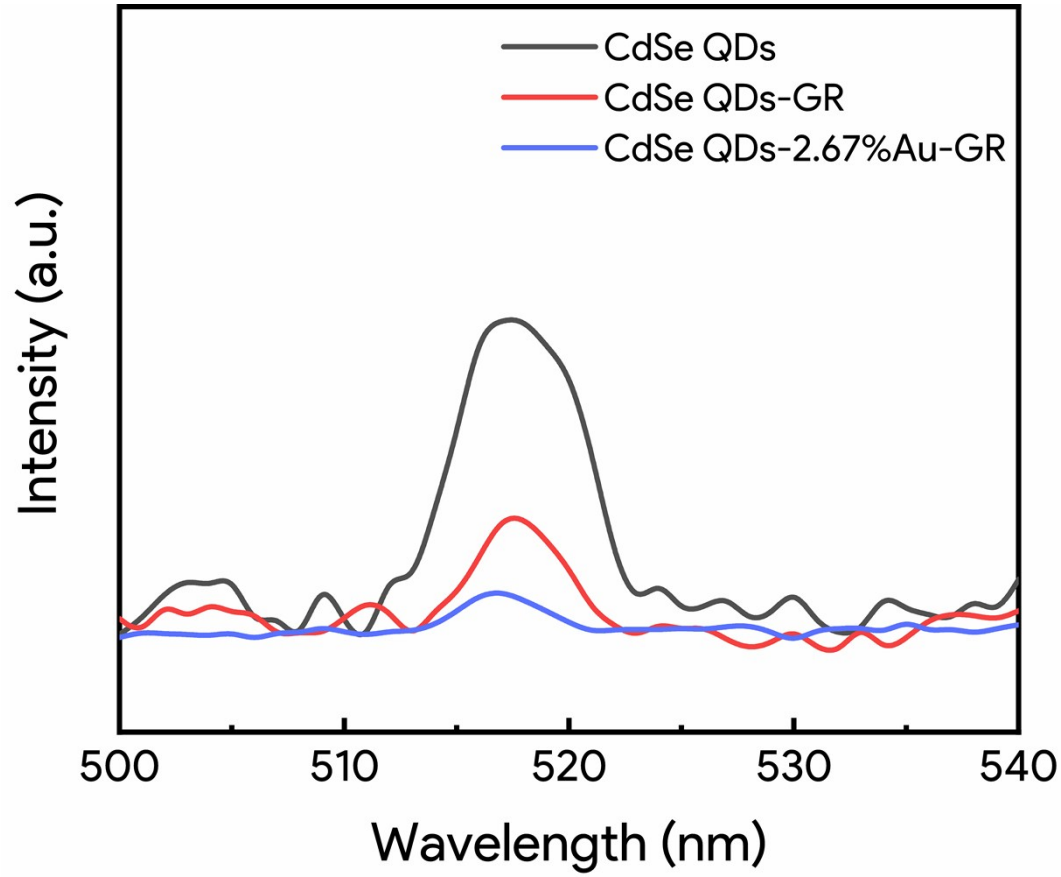

Fig. S23. PL results of blank CdSe QDs, CdSe QDs-GR, and CdSe QDs-2.67%Au-GR with an excitation wavelength of 380 nm.

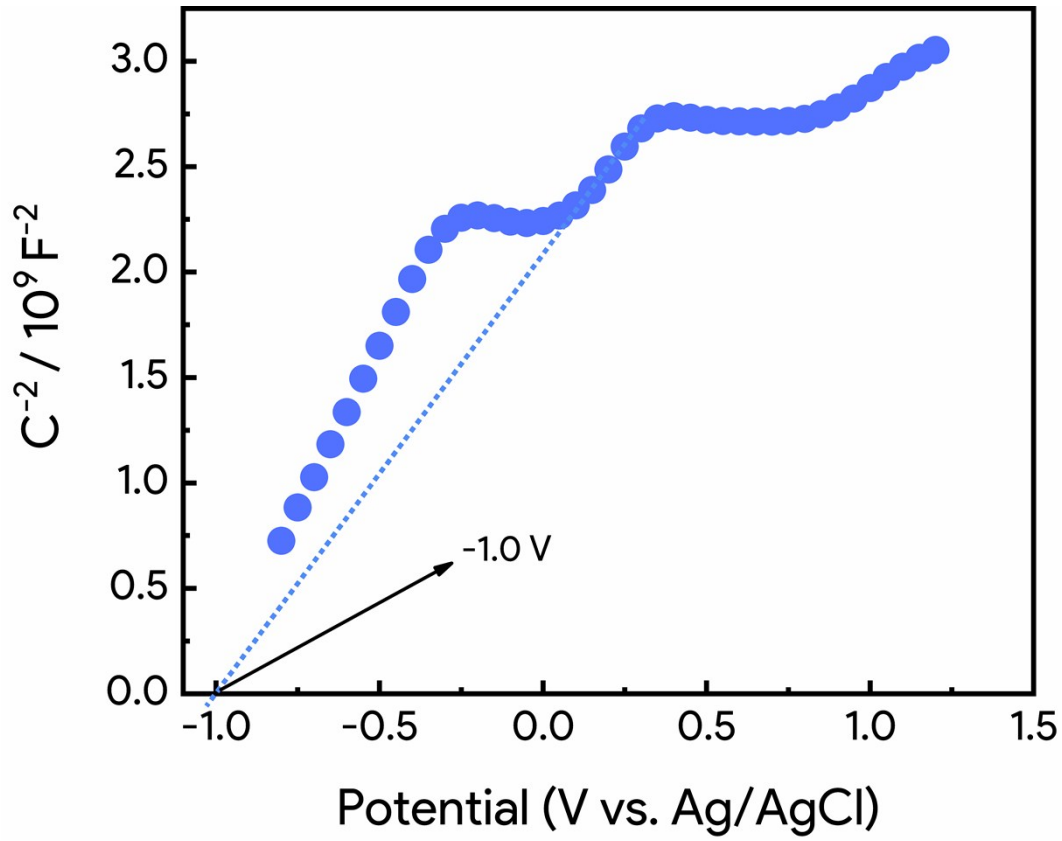

Fig. S24. Mott-Schottky result of CdSe QDs-2.67%Au-GR nanocomposite.

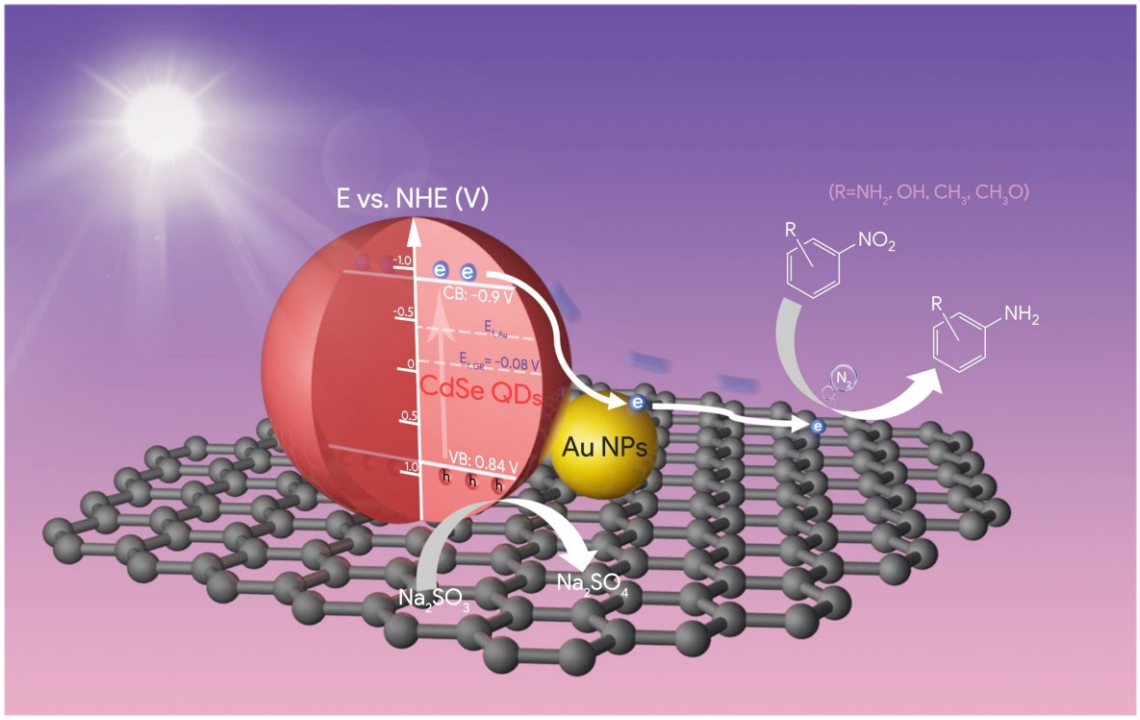

Scheme S1. Schematic illustration of the photocatalytic mechanism of CdSe QDs-Au-GR nanocomposites.

Note: According to the Mott−Schottky result (**Fig. S21**) of CdSe QDs-2.67%Au-GR nanocomposite, flat band potential (V_{fb}) of CdSe QDs ingredient in the optimal ternary nanocomposite was determined to be ca. −1.0 V vs Ag/AgCl, that is, −0.8 V vs NHE by the horizontal intercept of extrapolation along the linear part, by which the conductive band potential (V_{CB}) was determined to be ca. −0.9 V vs NHE.[1,2] On the other hand, considering the E_g value (1.74 eV) determined by the DRS result (**Fig. S7**), valence band potential (V_{VB}) of CdSe QDs in the nanocomposite can be calculated to be 0.84 V vs NHE based on the formula $E_g = V_{VB} - V_{CB}$. Owing to the favorable energy-level alignment, photoexcited electrons were rapidly transferred from the CB of CdSe QDs to the Au NPs in terms of the strong electronegativity and electron-trapping role of Au NPs, and then transferred to the intimately integrated GR layer ($E_{f,GR} = -0.08$ V vs NHE[3]), which greatly prolongs the lifetime of photogenerated electron-hole charge carriers, leading to superior photocatalytic performances.

References

1 M.-H. Huang, X.-C. Dai, T. Li, Y.-B. Li, Y. He, G. Xiao and F.-X. Xiao, *J. Phys. Chem. C*, 2019, **123**, 9721–9734.

2 N. Zhang, Y. Zhang, X. Pan, X. Fu, S. Liu and Y.-J. Xu, *J. Phys. Chem. C*, 2011, **115**, 23501–23511.

3 J. Zhang, F.-X. Xiao, G. Xiao and B. Liu, *Nanoscale*, 2014, **6**, 11293–11302.